Lab on a Chip

PAPER

View Article Online
View Journal

Cite this: DOI: 10.1039/c6lc00443a

Acoustofluidic actuation of *in situ* fabricated microrotors†

Murat Kaynak,[a] Adem Ozcelik,[a] Nitesh Nama,[a] Amir Nourhani,[b] Paul E. Lammert,[b] Vincent H. Crespi*[bcd] and Tony Jun Huang*[ae]

Received 3rd April 2016,
Accepted 18th July 2016

DOI: 10.1039/c6lc00443a

www.rsc.org/loc

We have demonstrated *in situ* fabricated and acoustically actuated microrotors. A polymeric microrotor with predefined oscillating sharp-edge structures is fabricated *in situ* by applying a patterned UV light to polymerize a photocrosslinkable polyethylene glycol solution inside a microchannel around a polydimethylsiloxane axle. To actuate the microrotors by oscillating the sharp-edge structures, we employed piezoelectric transducers which generate tunable acoustic waves. The resulting acoustic streaming flows rotate the microrotors. The rotation rate is tuned by controlling the peak-to-peak voltage applied to the transducer. A 6-arm microrotor can exceed 1200 revolutions per minute. Our technique is an integration of single-step microfabrication, instant assembly around the axle, and easy acoustic actuation for various applications in microfluidics and microelectromechanical systems (MEMS).

Introduction

Remotely powered and autonomous microrotors play an important role in microelectromechanical systems (MEMS),[1–4] biomedical engineering,[5–10] and biochemical applications.[11,12] They are used in lab-on-a-chip applications for mixing[13,14] and pumping,[15,16] or for studying the rheological properties of microdroplets or microparticles.[17,18] Simple fabrication and easy tunable actuation have the potential to significantly enhance the efficiency and performance of these micromotors.

In recent years, significant advances have been made in actuating microstructures by hydrodynamic force,[19] laser manipulation,[20,21] bacterial motion,[22–24] magnetic force,[6,14] chemical propulsion,[25,26] and acoustic waves.[27–29] Yue *et al.* fabricated laser-actuated microgears with rotation rates around 60 revolutions per minute (RPM) at 2 watts.[20] Their method enabled simple *in situ* fabrication of microstructures in various geometries inside microchannels. Applying laser for actuation provides precision but simultaneous manipulation of microgears would require multiple laser beams. Moon *et al.* fabricated polymer micromachines that rotate around a pre-fabricated micropillar driven by hydrodynamic force.[19] A fluid is injected in the microchannel, and a rotation rate of 5 RPM per 1 μL min^{-1} of fluid flow in a 200 μm wide channel is obtained. Di Leonardo *et al.* studied micromotors that use bacteria as a source of driving force.[23] These micromotors could rotate at 1 RPM with an unstable frequency. Lu *et al.* and Ahn *et al.* utilized magnetic actuation for micromixing[14] and micropumping,[6] which require magnetic components and relatively complex operational setups. Shilton *et al.* introduced micromotors driven by surface acoustic waves[27,28] and obtained high rotation rates with a drawback of laborious and expensive fabrication. A performance comparison of existing microrotors is given in Table S1.†

The aforementioned microrotors are encouraging and provide innovative approaches for generating rotary motion in small scale. However, further improvements in fabrication[6,14,27,28] and performance are necessary to improve the practicality and applicability of these microrotors.[20,21] Continuous or stop-flow UV polymerization techniques can yield complex microstructures for microfluidics in a simple fabrication.[19–21,30–32] However, easy actuation and high rotation rate are still needed for microrotors, micropumps, and microgears fabricated by UV polymerization. In the last decade, various microscale acoustofluidic technologies have demonstrated simple, low-cost, contactless, and versatile operations in lab-on-a-chip applications,[33–35] such as micropumps[36] and micromixers.[37–40] Acoustically oscillating sharp-edge structures, particularly, have been implemented for

[a] Department of Engineering Science and Mechanics, The Pennsylvania State University, University Park, PA 16802, USA. E-mail: junhuang@psu.edu; Fax: +814 865 9974; Tel: +814 863 4209
[b] Department of Physics, The Pennsylvania State University, University Park, Pennsylvania 16802, USA. E-mail: crespi@phys.psu.edu; Tel: +814 863 0163
[c] Department of Materials Science and Engineering, The Pennsylvania State University, University Park, PA 16802, USA
[d] Department of Chemistry, The Pennsylvania State University, University Park, Pennsylvania 16802, USA
[e] Department of Biomedical Engineering, The Pennsylvania State University, University Park, Pennsylvania, 16802 USA

† Electronic supplementary information (ESI) available: Supplementary Videos S1–S5, Fig. S1 and Table S1. See DOI: 10.1039/c6lc00443a

fluid mixing,[39,41] pumping,[36] sputum liquefaction,[36] and generation of chemical gradients.[42] In this work, we combine single-step fabrication with straightforward acoustofluidic actuation of microrotors. UV polymerization of microrotors around polydimethylsiloxane (PDMS) micropillars was used to fabricate complex microstructures. Piezoelectric transducers acoustically actuated oscillations of sharp-edge structures to generate microstreaming flows that in turn induce rapid rotation. This method has easy fabrication, remote actuation, and fine tunability. It could be used in various demanding microfluidic applications in biomedical, physical, and chemical fields.

Experimental methods

Fig. 1a shows the *in situ* fabrication scheme for acoustically actuated microrotors situated within microchannels. First, a single-layer PDMS microchannel (containing micropillars that act as axles) was fabricated using soft lithography and replica molding. We pretreated a silicon wafer with hexamethyldisilazane (HMDS), patterned in photoresist (Megaposit SPR955, Microchem, USA), and etched using deep reactive ion etching (DRIE). To reduce the surface energy of the silicon wafer and ease the peeling of the PDMS channel, we coated the silicon master with chlorotrimethylsilane (75-77-4, Alfa Aesar, USA). The PDMS microchannel was fabricated by curing a 10 : 1 mixture of PDMS resin and curing agent (Sylgard 184, Dow-Corning, USA) at 65 °C for 2 h. Then we peeled off the PDMS layer from the mold and used a reusable biopsy punch (Harris Uni-Core 0.75 mm) to punch holes for inlet and outlet. The PDMS channel is 100 μm deep and 2 mm wide in the region where UV polymerization and acoustic actuation occur. Later, we coated a glass slide (48404-454, VWR, USA) with PDMS using a spin coater (WS-650MZ-23NPP/Lite, Laurell Technologies, Czech Republic) at 1000 RPM for 1 minute, and baked at 65 °C for 30 min. The PDMS microchannel was bonded onto the PDMS coated glass slide and the whole device was baked at 65 °C for 2 h.

For *in situ* microrotor fabrication, a mercury lamp (Intense Light C-HGFI, Nikon, Japan) provided the white light source. A computer controlled mechanical shutter (LB-SC, Sutter Instrument Company, CA, USA) controlled UV exposure time, in our case 50 ms. An inverted microscope (Nikon TE-2000U) equipped with a 10× objective lens (Plan Fluor 10×/0.3 DIC L/N1, infinity/0.17 WD 16.0, Nikon, Japan) and a filter cube (11000v3: UV, Chroma) was used for *in situ* fabrication of microrotors into these channels. The UV light intensity exiting the 10× objective lens was measured as ~80 μW cm^{-1},[2] which was fixed in our experiments, using a power meter (FieldMaxII-TO Laser Power/Energy Meter, Coherent Inc., USA). The UV light, then, entered the microchannel and polymerized the intended microrotors. A transparent photomask containing the rotor design was placed into the field-stop slot of the microscope. A solution consisting of 40% (v/v) polyethylene glycol (PEG) diacrylate with a molecular weight of 700 (PEG700, Sigma-Aldrich, MO, USA), 25% (v/v) PEG with a molecular weight of 258 (PEG 258, Sigma-Aldrich, MO, USA), 15% (v/v) photoinitiator 2-hydroxy-2-methyl-1-phenyl-propan-1-one (Darocur

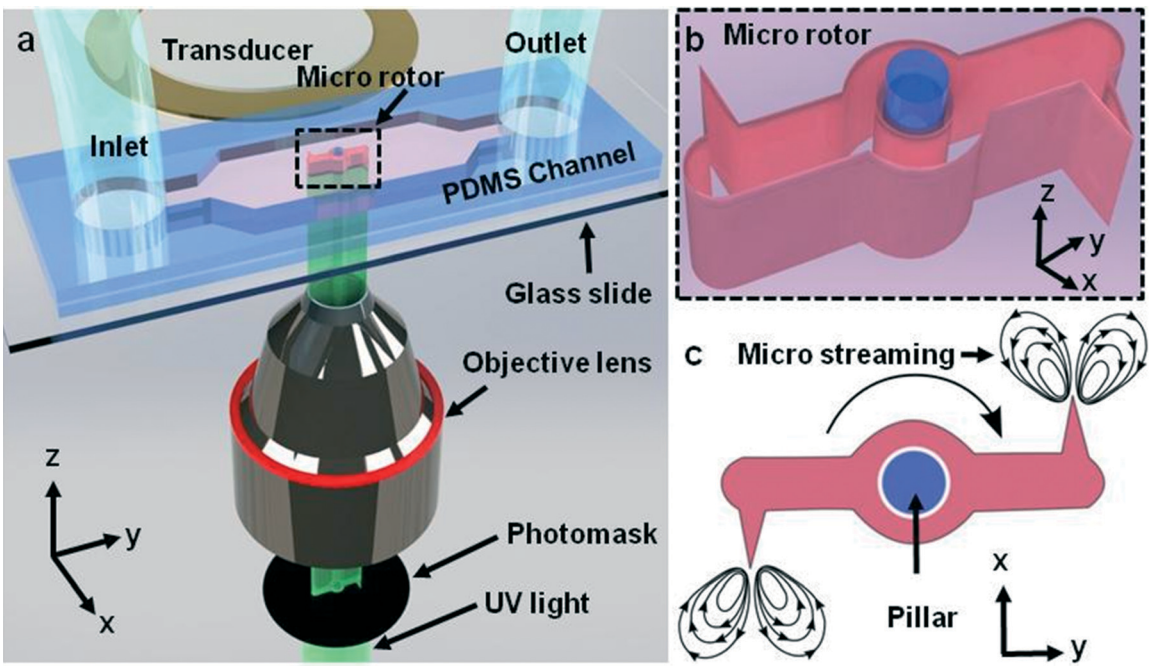

Fig. 1 (a) Schematic of fabrication and actuation setup (not to scale). A mask and an objective lens are used for patterning and focusing UV light. (b) Schematic of microrotor which is fabricated around existed PDMS pillar (diameter: 90 μm) and able to rotate freely. The depth of the fabricated microrotors is ~96 μm which is slightly smaller than the channel height due to the oxygen inhibition layers. (c) Schematic of acoustically actuated two-arm microrotor. The end-to-end distance and the inner diameter of the microrotor are 550 μm and 100 μm, respectively. When the acoustic field is present, sharp-edge structures oscillate and generate acoustic streaming, which rotates the microrotor.

1173, from Ciba), 15% (v/v) TE buffer (100 TE, from OmniPur), and 5% (w/v) Rhodamine 6G, was injected into the PDMS microchannel through the inlet by a 1 ml syringe (McKesson, CA, USA). After the injection we waited 5 minutes to ensure that solution flow inside the channel came to a full stop. The axle pillar and the rotor pattern in the photomask were then aligned concentrically. Upon UV exposure and polymerization, the microrotor forms *in situ* around the PDMS axle inside the microchannel (Video S1†). After fabrication, we washed away the unpolymerized solution in the microchannel with an ethanol solution, observing no significant shape deformation of the microrotor. Fig. 1b provides a perspective schematic view of a microrotor. The UV polymerized microrotor is able to rotate freely in an ethanol medium without adhering to the substrate or axle. PDMS is an oxygen-permeable material that forms a thin oxygen inhibition layer near the PDMS channel boundaries both at the bottom and the top, and constrains the PEG from UV-polymerizing near PDMS walls.[30,43–47]

For actuation, a piezoelectric transducer (81-7BB-27-4L0, Murata Electronics, Japan) was bonded next to the PDMS device (see Fig. 1a) on the same glass slide using a thin layer of epoxy (G14250, MA, USA). Activation of the piezoelectric transducer was controlled by sine-wave signals from a function generator (AFG3011, Tektronix, USA) amplified by an RF amplifier (25A250A, Amplifier Research, USA).

Results and discussion

We fabricated microrotors without and with sharp-edge structures on the same or opposite sides of microrotors to demonstrate the proof of the concept for rotational actuation, as shown in Fig. 2. The microstructure without sharp-edge structures (Fig. 2a and b) does not generate significant acoustic streaming and thus did not rotate under acoustic drive. When the sharp-edge structures are on the same side of the two-arm structure (Fig. 2c and d), there was no net rotation because the acoustic streaming cannot impose a net torque on this mirror-symmetric structure. On the other hand, when the sharp-edge structures are situated on opposite sides of the two-arm rotor (Fig. 2e–h), acoustic streaming produces a net torque on the microrotor and we obtained clockwise (CW) and counterclockwise (CCW) rotation. We can fabricate CW or CCW rotating microrotors with one photomask, simply by flipping the photomask in the field stop.

The angular speed of the microrotors was characterized as a function of the driving frequency. The maximum angular speed occurred near 4.3 ± 0.3 kHz which is slightly lower than the nominal resonant frequency of the transducer (4.6 kHz). However, as shown in Fig. S1a,† bonding the transducer to the glass slide lowers its resonant frequency to ~4.4 kHz which agrees reasonable well with the frequency of highest angular speed (Fig. S1b†).

Next, we investigated the effect of the number of arms on rotational performance, to determine whether the individual arms contribute additively, or if interactions between the streaming fields of nearby arms may enhance or degrade the overall performance of the device. All arms have the same size, with one sharp-edge structure on each trailing edge, as shown in Fig. 3a–f. Fig. 3g shows the performance of microrotors with from 1 to 6 arms (Video S2†). Due to geometrical

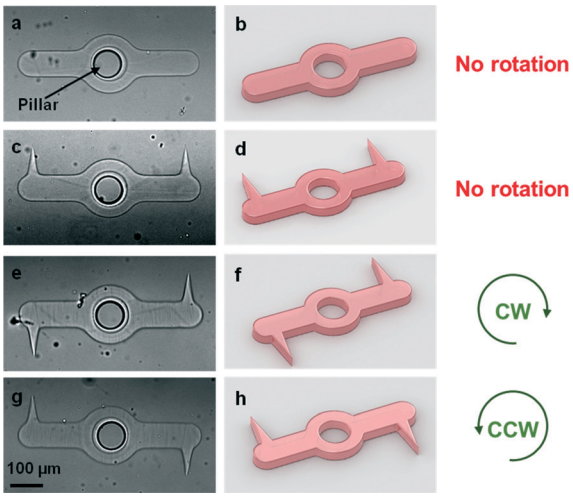

Fig. 2 Image and schematic of proof-of-concept, which illustrates the effect of sharp-edge structures on rotation. (a), (b) Image and schematic of 2-arm rotor without sharp-edge structure which is not supposed to rotate. (c), (d) Relative placement of sharp-edge structures results in cancelling torques. No rotation is expected. (e), (f) The microrotor rotates clockwise because of the position of sharp-edge structures, which creates a net torque from acoustic streaming. (g), (h) The microrotor rotates counter-clockwise due to the position of the sharp-edge structures.

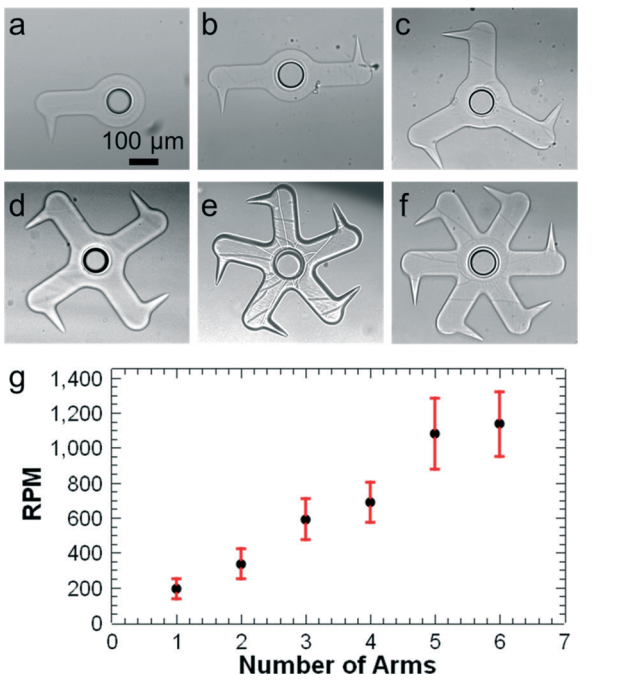

Fig. 3 Microrotors with different numbers of arms. (a)–(f) Images of 1-arm to 6-arm microrotors fabricated around existed pillar. (g) Angular speed *vs.* number of arms. With increasing number of arms around the pillar, angular speed increases because the more sharp-edge structures, the more acoustic streaming and force that can be generated. Error bars represent standard deviation of five or more repeated experiments.

constraints, we could not increase the number of arms beyond 6. The peak-to-peak voltage (V_{PP}) in Fig. 3g was fixed at 160 V_{PP} (the maximum voltage applied in this study). The angular velocity is nearly linear in the number of arms, varying from ~200 RPM for one arm to ~1200 RPM for six arms. If the propulsive contributions of individual arms are largely independent of each other, then this result suggests that the drag force on the rotor is largely independent of the number of arms, *i.e.*, arises predominately from the axle region. The similar sizes of the gaps between the axle and rotor and between the rotor surfaces and the top and bottom of the microchannel then suggest that the forces impeding rotation do not arise exclusively from viscous drag at these interfaces (otherwise, the drag on the arms would dominate). This conclusion is consistent with the threshold voltage necessary to initiate sustained motion being somewhat lower for the rotors with more arms. When the acoustic field was turned off, a 4-arm microrotor came to a full stop after 1.8 milliseconds and ~2 degrees of further rotation (Video S3†). This rapid slowdown is promising for applications that require discrete step-wise rotation.

The acoustic streaming is controlled by the amplitude of the transducer voltage, which provides straightforward tunability of the rotation rate. Fig. 4 shows the angular speed of an acoustically actuated 6-arm microrotor as a function of the applied peak-to-peak voltage from 40 V_{PP} to 160 V_{PP} (Video S4†). A parabolic relation here is consistent with the second-order nature of acoustic streaming, if one assumes that the overall velocity of the rotor structure scales linearly with the rate of momentum transfer from acoustic streaming and that the amplitude of sharp-edge structure motion is linearly proportional to the drive voltage. However, considering that the overall rotor motion is not in the limit of small Reynolds number (see below) and there is a modest threshold voltage needed to obtain sustained motion, one must also consider the possibility that the relation is more complex. Below 40 V_{PP} rotation was less than 6 RPM. Fig. 4a–f show one full clockwise rotation of the 6-arm microrotor at 100 V_{PP} divided into 6 frames, one rotation being completed in 108.5 milliseconds. As shown in Fig. 4g, the angular speed of an acoustically actuated 6-arm microrotor monotonically increases from ~550 RPM at 100 V_{PP} to ~1200 RPM at 160 V_{PP}.

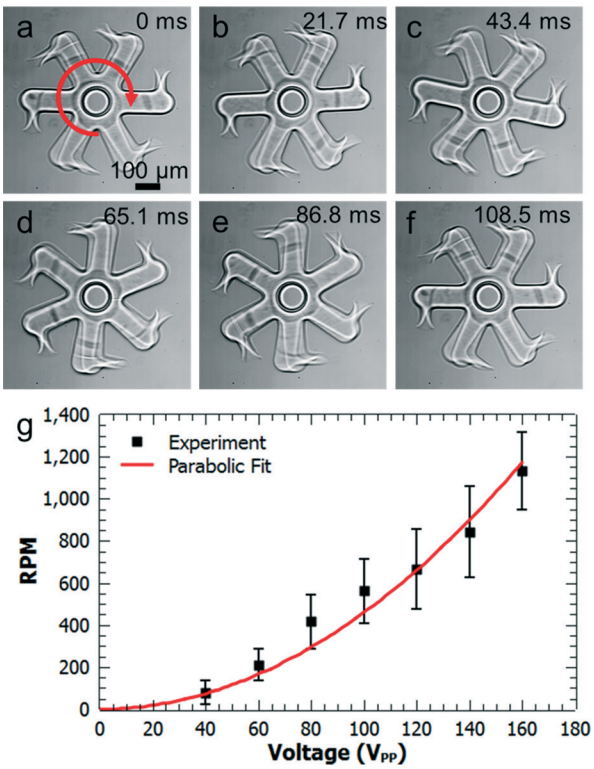

Fig. 4 (a)–(f) Image series for an acoustically actuated 6-arm microrotor, showing a full rotation across 6 frames. (g) RPM *versus* peak-to-peak voltage for a 6-arm microrotor, showing an increase of the angular speed with the applied voltage amplitude, above a small offset voltage (20–30 V) necessary to initiate motion. Error bars represent standard deviation of five or more repeated experiments. The coefficient of parabolic fit is 0.0458 RPM/V_{PP}^2.

As an application of the acoustically actuated microrotors, we have demonstrated mixing of two fluids using a 6-arm microrotor actuated at 160 V_{PP}. In this simple example, we injected ethanol solution with suspended fluorescent beads and pure ethanol into the microchannel at a total flow rate of 10 μl min^{-1}. Upon the application of acoustic field, the microrotor mixed the two fluids in under 30 milliseconds (Video S5†).

Mechanism

A linear system subjected to monochromatic sinusoidal actuation oscillates at the frequency of the driving force. Our microrotor systems are driven by an acoustic signal with a frequency of several kHz. The immediately observable responses are oscillation of the sharp-edge structures at the ends of the arms at the drive frequency (see Fig. 5) and steady rotation of the entire microrotor, which is really a zero-frequency motion because it is not oscillatory. This zero-frequency motion must be due to nonlinearities in the dynamics, and is very likely due to so-called acoustic streaming.[48,49] Acoustic streaming originates from dissipation in the fluid, either in the boundary layer (resulting in boundary-layer driven streaming) or in the bulk fluid. The relative contribution of these mechanisms to the mean flow generation depends on the size of the device. Since our device is much smaller than the inverse of the spatial damping rate, we expect weak interior dissipations in our device.[50] Thus, we believe the boundary-driven streaming to be the dominant mechanism in our devices. However, by retaining the bulk viscosity terms in our numerical formulation, we have considered both mechanisms of acoustic streaming in our numerical results. The acoustic streaming patterns are schematically depicted in Fig. 1c and are experimentally visualized in Fig. 5a with the aid of 1 μm diameter fluorescent tracer particles.

To numerically investigate the acoustic streaming, we followed the previously reported perturbation approach[48]

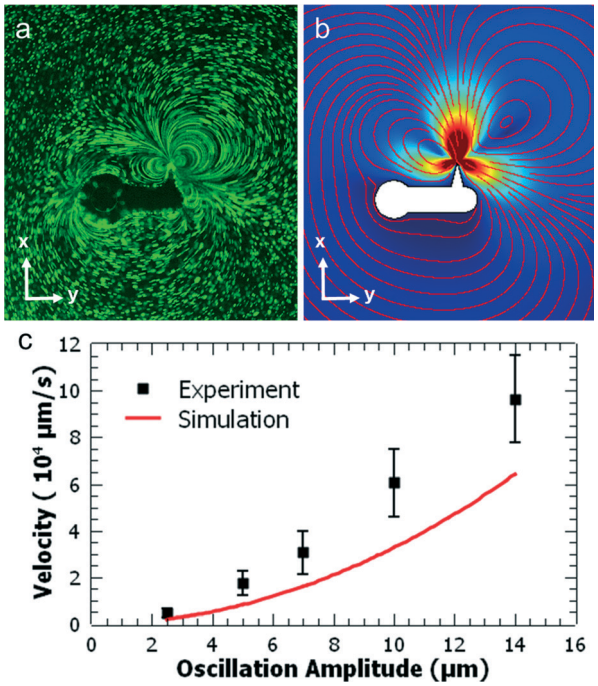

Fig. 5 Acoustic streaming patterns around oscillating of a one-arm structure. (a) Fluorescent microscopy images of 1 μm polystyrene beads are stacked to visualize the vortices. (b) Streaming flows are numerically produced using perturbation approach. (c) Experimental and numerical analysis of streaming velocities ~40 μm away from the tip along the *x* axis. The coefficient of the numerical curve is 0.0326 (μm s)$^{-1}$.

where we split the flow variables into first- and second-order components. Upon substitution into the balance laws, this results in two separate sets of first- and second-order equations which are then solved successively to predict the response of the fluid. Fig. 5b shows numerically computed particle trajectories which appear to be in good qualitative agreement with the observed flow patterns visualized in Fig. 5a. The non-symmetric nature of the streaming patterns around the tip of sharp-edge structure can be attributed to the inherent asymmetry in the geometry of the arm of the microrotor as well as a slight tilt of the sharp-edge structure that may result from the fabrication. Significant nonlinear effects indicate that the local Reynolds number should not be small. Reynolds number is a characteristic speed times a characteristic length divided by the fluid kinematic viscosity (UL/ν). It is precisely defined, but not often unique since different parts of a system (*e.g.*, sharp-edge structure, arm) may have different sizes and may move with different characteristic velocities. At 160 V_{PP}, oscillation of the 100 μm long sharp-edge structure is 100 μm peak-to-peak, giving an average tip speed of $U \approx 4 \times 10^5$ μm s^{-1}. With $L \approx 100$ μm, the length of sharp-edge structure, and $\nu = 1.5 \times 10^6$ (μm)^2 s^{-1}, the kinematic viscosity of ethanol, this motion corresponds to a Reynolds number of approximately 26. While this is the Reynolds number relevant to the streaming, it is interesting to note that the overall rotational motion is also not in the low-Reynolds number regime. At 1000 RPM, the end of the rotor that is 275 μm from the axle center has a speed of $U \approx 3 \times 10^4$ μm s^{-1}. With $L \approx 275$ μm, this gives a Reynolds number of about 5.5. The Reynolds number associated with the small gaps between the rotor and the upper and lower surfaces of the channel is proportionately smaller.

To experimentally characterize the streaming speeds for different values of tip displacement, we analyzed the motion of 1 μm diameter polystyrene beads. Fig. 5c shows a quantitative comparison between the experimentally measured and numerically predicted streaming speeds with a coefficient of 0.0326 (μm s)$^{-1}$ at a position 40 μm away from the tip of sharp-edge structure along the *x*-axis for different values of the tip displacement. The plot shows semi-quantitative agreement between the experiments and numerical simulations. The differences may be due to the structural imperfections or lack of precise knowledge of the vibrating profile of the sharp-edge structures. Nonetheless, the numerical model can predict the trends concerning with the effects of various geometrical and operational parameters on the acoustic streaming flow, and thus is useful for design and optimization. Both in experimental and numerical results, the streaming speeds scale quadratically with the vibrational amplitude, consistent with the streaming flow being second-order in the velocity (or equivalently, the displacement amplitude).[48,49]

Conclusion

We have demonstrated single-step *in situ* fabrication of microrotors using UV polymerization in a microchannel. The microrotors have sharp-edge structures that are positioned asymmetrically on the rotor crossbar. Piezoelectric transducers enable acoustofluidic actuation of the microrotor through streaming flows induced by the oscillations of sharp-edge structures. These acoustic streaming flows break reflection symmetry and thus induce a net torque on the rotor arm. The angular speed increases uniformly and nearly linearly with the number of arms, attaining the highest speed for six arms. The angular speed is also controlled by the peak-to-peak voltage applied to the transducer, achieving rates above 1200 RPM for the 6-arm microrotor driven at 160 V_{PP}. The simple fabrication and easy actuation of these microrotors makes them suitable for many potential applications (such as micropumps, micromixers, microgear systems, and micromachinery) in physics, biochemistry, and biomedical engineering.

Acknowledgements

We gratefully acknowledge financial support from National Institutes of Health (R01 GM112048 and R33 EB019785), National Science Foundation (IIP-1534645, CBET-1438126, and IDBR-1455658), and the Penn State Center for Nanoscale Science (MRSEC) under grant DMR-1420620. This work was completed in the Penn State University Materials Research Institute Nanofab Facility. Murat Kaynak and Adem Ozcelik acknowledge the support from Turkey's Ministry of National Education.

References

1 A. C. R. Grayson, R. S. Shawgo, A. M. Johnson, N. T. Flynn, Y. Li, M. J. Cima and R. Langer, *Proc. IEEE*, 2004, **92**, 6–21.
2 M. A. Unger, H.-P. Chou, T. Thorsen, A. Scherer and S. R. Quake, *Science*, 2000, **288**, 113–116.
3 A. Waldschik and S. Büttgenbach, *Microsyst. Technol*, 2010, **16**, 1581–1587.
4 K. S. Ryu, K. Shaikh, E. Goluch, Z. Fan and C. Liu, *Lab Chip*, 2004, **4**, 608–613.
5 W. C. Chang and D. W. Sretavan, *Clin. Neurosurg*, 2007, **54**, 137–147.
6 C. H. Ahn and M. G. Allen, in *Proceedings IEEE Micro Electro Mechanical Systems*, 1995, IEEE, p. 408.
7 R. Nosrati, A. Driouchi, C. M. Yip and D. Sinton, *Nat. Commun.*, 2015, **6**, 8703.
8 L. Eamer, R. Nosrati, M. Vollmer, A. Zini and D. Sinton, *Biomicrofluidics*, 2015, **9**, 044113.
9 J. Kim, H. L. Ennis, T. H. Nguyen, X. Zhuang, J. Luo, J. Yao, R. H. Kessin, M. Stojanovic and Q. Lin, *Sens. Actuators, A*, 2012, **188**, 312–319.
10 S. Rozhok, C.-F. Shen, P.-L. Littler, Z. Fan, C. Liu, C. Mirkin and R. Holz, *Small*, 2005, **1**, 445–451.
11 Y. Xie, D. Ahmed, M. I. Lapsley, S.-C. S. Lin, A. A. Nawaz, L. Wang and T. J. Huang, *Anal. Chem.*, 2012, **84**, 7495–7501.
12 A. J. Chung, D. Kim and D. Erickson, *Lab Chip*, 2008, **8**, 330–338.
13 Y. Kim, J. Lee and S. Kwon, *J. Micromech. Microeng.*, 2009, **19**, 105028.
14 L.-H. Lu, K. S. Ryu and C. Liu, *J. Microelectromech. Syst.*, 2002, **11**, 462–469.
15 M. Sen, D. Wajerski and M. Gad-el-Hak, *J. Fluids Eng.*, 1996, **118**, 624.
16 S. G. Darby, M. R. Moore, T. A. Friedlander, D. K. Schaffer, R. S. Reiserer, J. P. Wikswo and K. T. Seale, *Lab Chip*, 2010, **10**, 3218.
17 Y. Hatwalne, S. Ramaswamy, M. Rao and R. A. Simha, *Phys. Rev. Lett.*, 2004, **92**, 118101.
18 A. Tokarev, A. Aprelev, M. N. Zakharov, G. Korneva, Y. Gogotsi and K. G. Kornev, *Rev. Sci. Instrum.*, 2012, **83**, 065110.
19 B.-U. Moon, S. S. H. Tsai and D. K. Hwang, *Microfluid. Nanofluid.*, 2015, **19**, 67–74.
20 T. Yue, M. Nakajima, M. Takeuchi and T. Fuku, *Int. J. Adv. Robot. Syst.*, 2014, **11**, 1.
21 T. Yue, M. Nakajima, M. Ito, M. Kojima and T. Fukuda, in *2011 IEEE/RSJ International Conference on Intelligent Robots and Systems*, IEEE, 2011, pp. 433–438.
22 A. Sokolov, M. M. Apodaca, B. A. Grzybowski and I. S. Aranson, *Proc. Natl. Acad. Sci. U. S. A.*, 2010, **107**, 969–974.
23 R. Di Leonardo, L. Angelani, D. Dell'Arciprete, G. Ruocco, V. Iebba, S. Schippa, M. P. Conte, F. Mecarini, F. De Angelis and E. Di Fabrizio, *Proc. Natl. Acad. Sci. U. S. A.*, 2010, **107**, 9541–9545.
24 Y. Hiratsuka, M. Miyata, T. Tada and T. Q. P. Uyeda, *Proc. Natl. Acad. Sci. U. S. A.*, 2006, **103**, 13618–13623.
25 G. Loget and A. Kuhn, *Nat. Commun.*, 2011, **2**, 535.
26 A. Nourhani, P. E. Lammert, V. H. Crespi and A. Borhan, *Phys. Fluids*, 2015, **27**, 012001.
27 R. J. Shilton, N. Glass, S. Langelier, P. Chan, L. Y. Yeo and J. R. Friend, *Proc. SPIE 8204*, ed. S. Juodkazis and M. Gu, 2011, p. 82041J.
28 R. J. Shilton, N. R. Glass, P. Chan, L. Y. Yeo and J. R. Friend, *Appl. Phys. Lett.*, 2011, **98**, 254103.
29 D. Ahmed, M. Lu, A. Nourhani, P. E. Lammert, Z. Stratton, H. S. Muddana, V. H. Crespi and T. J. Huang, *Sci. Rep.*, 2015, **5**, 9744.
30 S. E. Chung, J. Kim, S. E. Choi, L. N. Kim and S. Kwon, *J. Microelectromech. Syst.*, 2011, **20**, 785–787.
31 S. E. Chung, W. Park, H. Park, K. Yu, N. Park and S. Kwon, *Appl. Phys. Lett.*, 2007, **91**, 041106.
32 H. Kim, J. Ge, J. Kim, S. Choi, H. Lee, H. Lee, W. Park, Y. Yin and S. Kwon, *Nat. Photonics*, 2009, **3**, 534–540.
33 X. Ding, P. Li, S.-C. S. Lin, Z. S. Stratton, N. Nama, F. Guo, D. Slotcavage, X. Mao, J. Shi, F. Costanzo and T. J. Huang, *Lab Chip*, 2013, **13**, 3626.
34 H. Wang, Z. Liu, S. Kim, C. Koo, Y. Cho, D.-Y. Jang, Y.-J. Kim and A. Han, *Lab Chip*, 2014, **14**, 947.
35 D. Ahmed, A. Ozcelik, N. Bojanala, N. Nama, A. Upadhyay, Y. Chen, W. Hanna-Rose and T. J. Huang, *Nat. Commun.*, 2016, **7**, 11085.
36 P.-H. Huang, N. Nama, Z. Mao, P. Li, J. Rufo, Y. Chen, Y. Xie, C.-H. Wei, L. Wang and T. J. Huang, *Lab Chip*, 2014, **14**, 4319–4323.
37 D. Ahmed, X. Peng, A. Ozcelik, Y. Zheng and T. J. Huang, *AIP Adv*, 2015, **5**, 097161.
38 D. Ahmed, H. S. Muddana, M. Lu, J. B. French, A. Ozcelik, Y. Fang, P. J. Butler, S. J. Benkovic, A. Manz and T. J. Huang, *Anal. Chem.*, 2014, **86**, 11803–11810.
39 P.-H. Huang, Y. Xie, D. Ahmed, J. Rufo, N. Nama, Y. Chen, C. Y. Chan and T. J. Huang, *Lab Chip*, 2013, **13**, 3847–3852.
40 A. Ozcelik, D. Ahmed, Y. Xie, N. Nama, Z. Qu, A. A. Nawaz and T. J. Huang, *Anal. Chem.*, 2014, **86**, 5083–5088.
41 N. Nama, P.-H. Huang, T. J. Huang and F. Costanzo, *Biomicrofluidics*, 2016, **10**, 024124.
42 P.-H. Huang, C. Y. Chan, P. Li, N. Nama, Y. Xie, C.-H. Wei, Y. Chen, D. Ahmed and T. J. Huang, *Lab Chip*, 2015, **15**, 4166–4176.
43 D. Dendukuri, P. Panda, R. Haghgooie, J. M. Kim, T. A. Hatton and P. S. Doyle, *Macromolecules*, 2008, **41**, 8547–8556.
44 D. C. Pregibon, M. Toner and P. S. Doyle, *Langmuir*, 2006, **22**, 5122–5128.
45 P. Panda, S. Ali, E. Lo, B. G. Chung, T. A. Hatton, A. Khademhosseini and P. S. Doyle, *Lab Chip*, 2008, **8**, 1056.
46 M. Li, M. Humayun, J. A. Kozinski and D. K. Hwang, *Langmuir*, 2014, **30**, 8637–8644.
47 C. Decker and A. D. Jenkins, *Macromolecules*, 1985, **18**, 1241–1244.
48 N. Nama, P.-H. Huang, T. J. Huang and F. Costanzo, *Lab Chip*, 2014, **14**, 2824.
49 N. Nama, R. Barnkob, Z. Mao, C. J. Kähler, F. Costanzo and T. J. Huang, *Lab Chip*, 2015, **15**, 2700–2709.
50 J. Vanneste and O. Bühler, *Proc. R. Soc. A*, 2011, **467**, 1779–1800.

